Heliyon 9 (2023) e20262

Contents lists available at ScienceDirect

Heliyon

journal homepage: www.cell.com/heliyon

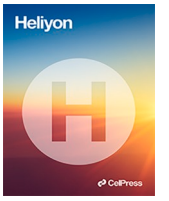

Tailored spectroscopic characteristics of a new type of CuO nanoparticles-inserted borate glass system: Samarium concentration tuning effect

I. Abdullahi [a,b], S. Hashim [a,*], S.K. Ghoshal [a], M.I. Sayyed [a,c]

[a] Department of Physics, Universiti Teknologi Malaysia, 81310 Skudai, Johor, Malaysia
[b] Department of Physics Federal University Gusau, Zamfara State Nigeria
[c] Department of Physics, Faculty of Science, Isra University, Amman, Jordan

ARTICLE INFO

Keywords:
Luminescence
Glasses
Samarium
Nanoparticles
Judd-ofelt

ABSTRACT

The demand for new glass hosts with emergent properties is constantly growing for various miniaturized applications. Thus, some new types of Sm_2O_3-activated strontium-telluro-alumino-magnesium-borate glasses with copper oxide nanoparticles (CuONps) insertion were made using melt-quenching approach. The obtained glasses were characterized to determine the effects of Sm_2O_3 concentration changes on their thermal, structural, and luminescence properties. XRD, FTIR, and HRTEM analyses of the samples verified their glassy nature, presence of different functional units and CuONps, respectively. DTA analysis showed excellent thermal stability of these glasses with a stability factor as much as 125 °C. The optical absorption properties of the glasses were highly sensitive to Sm^{3+} concentrations variation. The Judd-Ofelt intensity parameters of the glasses with and without CuONps followed the trend of $\Omega_6>\Omega_4>\Omega_2$ and $\Omega_4>\Omega_6>\Omega_2$, respectively. These glasses displayed 4 visible luminescence bands at 561, 598, 645, and 705 nm corresponding to $^4G_{5/2} \rightarrow {}^6H_{5/2}$, $^4G_{5/2} \rightarrow {}^6H_{7/2}$, $^4G_{5/2} \rightarrow {}^6H_{9/2}$, and $^4G_{5/2} \rightarrow {}^6H_{11/2}$ transitions in Sm^{3+}. In addition, branching ratio above 80% and stimulated emission cross-section up to 135.82×10^{-23} cm^2 were achieved. The stimulated emission cross-section and optical gain were enhanced due to the inclusion of CuONps in the glasses. These glasses may be useful for solid state laser and optical amplifier development.

1. Introduction

Particularly, in conventional and advanced technological applications based on luminescence properties, various rare earth ions (REIs)-activated glasses became a fundamental part. Owing to their well-shielded 4f orbitals, REIs display unique and superb optical attributes, such as enhanced absorption and emission cross-sections, extended luminescence lifetimes, and narrow spectral bandwidths [1–4]. These properties have been broadly studied and utilized in different scientific fields, for example, optics, photonics, and optoelectronics. Incorporating REIs into glassy hosts has led to the emergence of advanced optical materials with tunable properties [5, 6]. Solid-state laser development is one of the most significant contributions of REIs-doped glasses. The application of advanced solid-state lasers is found in the modern industries, health and pharmaceutical related fields, and in advanced research techniques

* Corresponding author.
E-mail address: suhairul@utm.my (S. Hashim).

https://doi.org/10.1016/j.heliyon.2023.e20262
Received 19 June 2023; Received in revised form 11 September 2023; Accepted 17 September 2023
Available online 19 September 2023

thanks to their high efficiency, compact size, and durability. In addition, the REI's' electronic energy levels have the ability to efficiently absorb and emit light at specific wavelengths, which is why they are ideal for use in lasers, lightning, and displays.

REIs-activated glasses are preferred for diverse lighting and displays due to their high thermal and chemical stability, easy manufacturing, and low cost. However, it was proven that the luminescence efficiency of the REIs is heavily dependent on the selected host matrix in which they are doped [7]. The host matrix affects the spectroscopic properties of the REIs by modifying their local environments, such as their crystal field, coordination number, and symmetry. This results in changes in the transition probabilities and, thus, the nature of transitions between manifold energy levels of the REIs, which in turn affect their luminescence properties, such as the intensity, lifetime, and emission wavelength. Moreover, the host matrix can also affect the physical and optical attributes of the REIs. The host matrix can also affect properties such as refractive index, band gap energy, and density, which are important for optimizing photonics and other optical materials. For example, a high refractive index can increase the light emission's efficiency, infrared laser potency, and imaging quality, as reported by Lin et al., Zang et al., and Wang et al. [8–10]. It has been shown that optical glasses with high linear and nonlinear refractive indices have several advantages such as more efficient light focusing in lenses as well as optimizing the design of compact optical systems for photonic applications in the THz region, wide range of application in visible-infrared regions, optical filters and modulators, optical memory devices and laser windows, and optical switching cum signal processing [11–13]. Furthermore, high density can improve the compactness and durability of the material [14].

The selected oxide glass host play a paramount role in the design and optimization of high-performance REIs-doped optical glasses [7]. Silica, phosphate, borate, and tellurite are the typical REIs host matrices characterized by certain merits and demerits. However, the main drawback is the luminescence quenching effect; thus, the challenge of synthesizing an optimized REIs glass host with minimal inefficiencies still exists. Strontium-borate glasses are a class of glasses that have gained significant attention in recent years due to their potential for use in optical applications. The main constituents of these glasses were boron oxide (B_2O_3) and strontium oxide (SrO), as well as other elements that are added as either modifiers or dopants for tuning the properties of the glasses.

The unique composition of strontium-borate glasses allows for a wide range of optical and electronic properties to be achieved; this makes them appealing for applications such as lasers and luminescence due to lofty quantum efficiency, resistance to corrosion, reduced phonon energy ($\approx$1120 cm^{-1}), high refractive index ($\approx$2.89), high thermal expansion ($T_g \approx 376$ °C at $T_d = 341$ °C), and broad transmittance window in the ultra-violet and infrared zones [15–19]. According to many reports in literature, the introduction of heavy metal oxides (HMO) such as SrO into borate glass network reduces the phonon energy because of the SrO stimulated conversion of BO_3 into BO_4 units [20–23]. Additionally, low phonon energy in strontium containing borate glasses was linked to the reduced phonon frequencies of the HM-O vibrations in the glass and this in turn enhances the radiative decay of the doped rare earth ions [24]. For example, Khan et al. reported the lasing attributes of barium-incorporated strontium-borate glasses [16]. In the report, the authors reported an improved refractive index, optical gain, and attenuation of the REIs covalency; though the glasses were recommended for laser applications, the concentration quenching effect manifested beyond Sm_2O_3 contents of 0.5 mol%. Again, zinc-added strontium-borate glass hosts were developed through a conventional melt-quenching approach, and the glasses were endorsed for optical fiber applications because of their excellent optical absorption characteristics [25]. However, the photoluminescence emission exploration of the glass system was not conducted. Incorporation of Sm_2O_3 as dopants in strontium-borate glasses turned out to be a promising strategy for optical materials advancement. Among the REIs, Sm^{3+} has been shown to exhibit strong luminescence properties. At the same time, CuO nanoparticles have unique optical and electronic properties, including strong absorption and emission of light in the visible region [26,27]. By routing these two elements in a multicomponent strontium-borate glass host, it is possible to create a novel material with enhanced luminescence and lasing properties.

Based on the importance of REIs-doped oxide glass hosts, in this study, few strontium-telluro-alumino-magnesium-borate glass samples at various concentrations of Sm_2O_3 doping and fixed concentration of copper oxide nanoparticles inclusion were made via the melt-quenching method. Earlier, we reported the influence of Dy^{3+} activation on the upconversion luminescence traits of the developed hosts [28]. Herein, the proposed glasses were characterized to evaluate the influence of Sm^{3+} concentration changes on their thermal, physical, optical and spectroscopic properties. The developed glasses were shown to be promising for the development of optical amplifiers and solid-state lasers. It was asserted that the luminescence characteristics and stimulated emission cross-section of these glasses can be tailored by varying Sm_2O_3 doping contents and copper oxide nanoparticles embedment. TeO_2 was introduced into the glass constituents owing to its high refractive index and low phonon energy, thereby promoting radiative processes of rare earth ions doped glasses [29]. Moreover, the fragility of the Te–O bond enables rare earth ions to enter the glass network and be completely soluble easily. As an enhancer of optical attributes, compactness, and chemical durability of glass matrices, Al_2O_3 was also added [30,31]. Magnesium oxide as a modifier considerably reduces the crystallization rate of the glass melt [32].

2. Materials and methods

Glasses with the nominal composition (69-x)B_2O_3–20$SrCO_3$–7TeO_2–3Al_2O_3–1MgO-xSm_2O_3 were developed by employing melt-quenching technique wherein x ranges from 0.5 to 1.5 mol%. We reported the preparation procedure and the details of the $SrCO_3$, B_2O_3, TeO_2, MgO, Sm_2O_3, and CuO nanoparticles commercial powdered starting reagents elsewhere [33]. To determine the glass stability, differential thermal analysis was conducted using detector DTG-60H detector with serial number C30575500539TK from 25 to 1000 °C. Similarly, X-ray diffraction (10–100°), energy dispersive X-ray (120 kV), Fourier transform infrared (500–3000 cm^{-1}), high-resolution transmission electron microscope (120 kV), ultraviolet–visible–infrared absorption (200–1800 nm), and photoluminescence emission (450–750 nm) analyses were also carried out to unravel the influence of varying the Sm_2O_3 contents and copper oxide nanoparticles embedment. Furthermore, The Sm_2O_3 composition of the glass sample with the most intense photoluminescence emission was used in developing the glass embedded with copper oxide nanoparticles wherein 0.05 mol% Copper oxide nanoparticles

were introduced into the glass. The details of the glass compositions are presented in Table 1.

3. Results and discussion

3.1. Thermal parameters

The DTA analysis is a robust technique primarily used to unravel the heat flow's nature as a temperature function using two temperature variables: the endothermic glass transition temperature (T_g)and the exothermic crystallization temperature (T_c). From this set of temperatures, the glass stability factor ($\Delta T = T_c - T_g$) could be obtained. The degree of thermal stability against crystallization depends on the achieved values; magnitudes of $\Delta T > 100$ °C indicate a better glass-forming ability [34]. Fig. 1 shows the traced DTA thermograms of the synthesized glass samples, whereas Table 2 presents the achieved values of T_g and T_c together with the stability factor. For the 0.5 mol% Sm doped glass sample (BSm1), the T_g and T_c values were found to be 592 and 710 °C, respectively. These values yielded a glass stability factor of 118 °C, and the higher value of ΔT attested to the good thermal stability of the glass sample. However, as the Sm_2O_3 contents were increased to 0.7 mol% corresponding to the BSm2 glass sample, a new set of T_g and T_c were generated (594 and 714 °C, respectively), increasing the stability factor to 120 °C. The stability factor continuously increased with the Sm_2O_3 contents (except for BSm4 glass). The observed trend affirmed the role of Sm^{3+} doping in enhancing the glass's thermal stability by forming more Sm–O bonds. Li et al. and Vijayasri et al. reported the same observation regarding Sm^{3+} activated strontium aluminate glasses and Tb^{3+} doped strontium zinc borate glasses aimed at green laser applications, respectively [35,36]. Since the glass transition temperature is responsive to the average coordination number of the network forming atoms along with the generation of non-bridging oxygens [37], the witnessed change in the magnitudes herein suggests the formation of more non-bridging oxygen and BO_3/BO_4 units as well. The higher thermal stability of the current glass systems indicates the capability to resist the crystallization process during heating, an essential feature for the development of high performance lasers [38,39]. Analogously, introducing copper oxide nanoparticles increased the thermal stability of the glass samples.

3.2. Structural analysis

3.2.1. XRD profile

For the local structural probe, the XRD pattern of BCSm3 is shown in Fig. 2. The amorphous and disordered nature of the produced glass samples was justified and validated due to the absence of long-range ordered atomic arrangements typical for crystalline phases.

3.2.2. FTIR spectra

FTIR spectra were recorded and exhibited in Fig. 3 to probe the properties of the synthesized glasses' local structure. The spectra were dominated by the fundamental absorption bands of borate units in addition to other units. The microscopic boron-oxygen network combines a three-dimensional arrangement of trigonal BO_3 or tetrahedral BO_4 groups [40]. Chen et al. argued that the IR frequency peaks appearing in 1500–3000 cm^{-1} range are due to hydroxyl O–H and OH groups [14]. Thus, the observed bands at 2854 and 2926 were assigned to the stretching oscillations of O–H bonds. Similarly, the 1666 and 1645 cm^{-1} peaks were allotted to water molecules' H–*O*–H bending and O–H bonding vibration, respectively [41]. Moreover, since the peaks spanning from 1500 to 1200 cm^{-1} and 1086 are due to asymmetric stretching of B–O bonds [42], the frequency peak positioned at 1328 cm^{-1} was assigned to the oscillations of trigonal BO_3 groups and that at 1460 cm^{-1} is due to the vibrations of $–O_2BSr$. The appeared 684 cm^{-1} band was assigned to the bending oscillation of B–O–B linkages due to the conversion of BO_3 to BO_4 unit, while the frequency band at 1010 cm^{-1} may be ascribed to the anti-symmetrical lengthening of B–O bond in the borate unit with the tetrahedral arrangement (BO_4) [43]. The 684 cm^{-1} peak was more intense at Sm_2O_3 content of 1.0 and 1.2 mol%, respectively; this indicates the transformation of more BO_3 to BO_4 groups. The reformation of BO_3trigonal to BO_4tetragonal units through the production of non-bridging oxygen confirmed the existence of structural modifications within the glass samples in response to varying the contents of the introduced dopants. Hence, the glass's rigidity and compactness were modified. Furthermore, based on the description of Ergene et al. that the frequency bands spanning 600 to 1000 cm^{-1} are characteristic vibrations of Al–O bonds [44]; the 684 cm^{-1} band may also be allocated to the Al–O bond herein. The details of the bands positions and their corresponding assignments were presented in Table 3. The changes in the intensities of the observed IR bands, resulting from modifications in both the concentration of Sm^{3+} and the incorporation of copper oxide nanoparticles, provided evidence of local structural rearrangement within the glass network.

Table 1
Details of the compositions and codes of the developed glasses.

Glass name	Composition (mol%)						
	B_2O_3	$SrCO_3$	TeO_2	Al_2O_3	MgO	Sm_2O_3	CuO Nps
BSm1	68.5	20	7	3	1	0.5	–
BSm2	68.3	20	7	3	1	0.7	–
BSm3	68.0	20	7	3	1	1.0	–
BSm4	67.8	20	7	3	1	1.2	–
BSm5	67.5	20	7	3	1	1.5	–
BCSm3	68.0	20	7	3	1	1.0	0.05

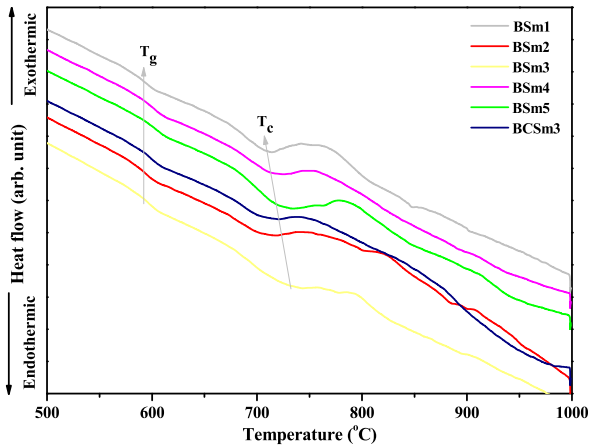

Fig. 1. DTA thermograms of the produced glasses.

Table 2
The transition temperature (T_g), crystallization temperature (T_c), and stability factor (ΔT) of the synthesized glasses.

Glass code	T_g (°C)	T_c (°C)	$\Delta T = T_c - T_g$ (°C)
BSm1	592	710	118
BSm2	594	714	120
BSm3	596	718	122
BSm4	595	715	120
BSm5	594	719	125
BCSm3	593	718	125

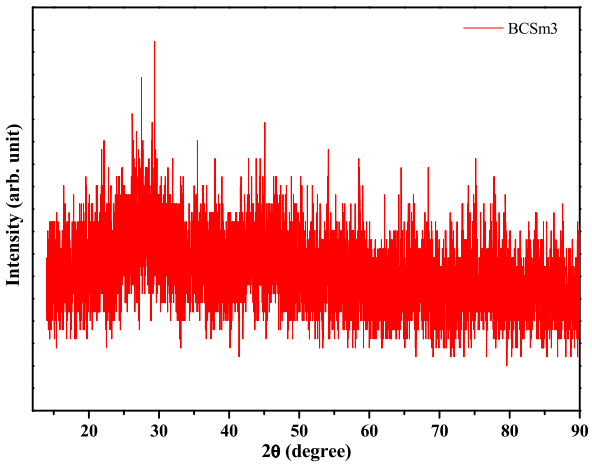

Fig. 2. XRD pattern of BCSm3 glass sample.

3.2.3. EDX spectra and HRTEM micrographs

The EDX maps of the traced elements are exhibited in Fig. 4a–g wherein the existence of strontium, tellurium, aluminium, magnesium, samarium, boron, and copper, respectively was revealed. The elements were traced along their characteristics K_α and L_α lines, respectively. It was verified that the EDX detector yielded a uniform spatial distribution of the individual elements. This observation suggests that the glasses were synthesized under optimal conditions with uniform incorporation of the elements. Uniform elemental distribution within the glass samples is essential for achieving optimal luminescence properties of rare-earth-doped systems as it warrants to consistent and uniform emission. Furthermore, the existence of dispersed copper oxide nanoparticles was confirmed and validated from the HRTEM frame displayed in Fig. 5a whereas Fig. 5b revealed the histogram of the nanoparticles size distributions. The visualized nanoparticles are of various dimensions and spherically shaped, with an average diameter size of 14 nm.

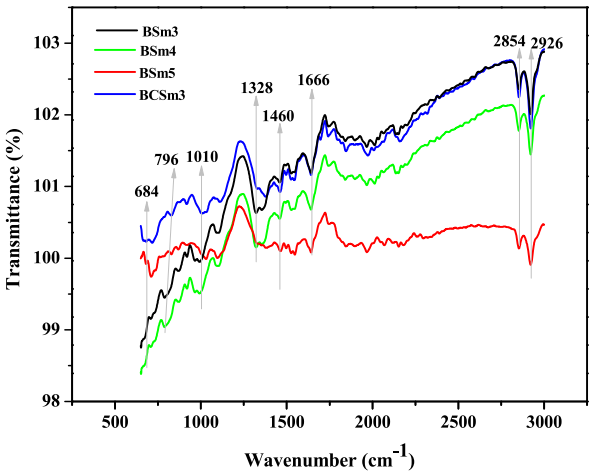

Fig. 3. FTIR spectra of the fabricated glass samples.

Table 3
FTIR bands and their assignments.

Band peak (cm^{-1})	Band assignment
684	Vibrations of B–*O*–B linkages or Al–O bonds [43,44]
796	B–O stretching vibrations in BO_4 groups [45]
1010	asymmetrical stretching of B–O bond in BO_4 units [43]
1328	oscillations of trigonal BO_3 groups [42]
1460	vibrations of $–O_2BSr$ [42]
1666	H–*O*–H bending of water molecules [41]
2854	Stretching oscillation of O–H bonds [14]
2926	Stretching oscillation of O–H bonds [14]

3.2.4. Density, molar volume, and ionic concentration

The densities, molar volumes, and ionic concentrations of the fabricated glasses were furnished in Table 4; the density values were obtained using Archimedes's principle with toluene as the liquid in accordance with the theoretical formulations outlined in Ref. [46]. As the Sm_2O_3 content in the glass samples was raised to 1.0 mol%, the density of the glass samples gradually enhanced (2.79, 2.82, and 2.84 g cm^{-3}, respectively), and then decreased with further addition of the dopant (2.84 and 2.85 g cm^{-3}). An analogous observation was reported by Al-Nidawi et al. regarding the boron oxide-added ZnO–SiO_2 glass matrix [47]. However, introducing copper oxide nanoparticles saw the enhancement of the density value to 2.84 g cm^{-3}. The increase in the density of the glass samples with increasing Sm_2O_3 contents may be linked to the denser nature of Sm_2O_3 (348.7 g mol^{-1}) in comparison with B_2O_3 (69.6 g mol^{-1}) and that Sm_2O_3 is being introduced into the glass at the expense of B_2O_3. Whilst the attenuation of the density may be explained by the growth and generation of new bonds resulting in the slight structural relaxation within the glass network [47], the irregular variation in the density pattern may be linked to the modifications in the coordination number and geometrical configuration as confirmed from the FTIR analysis. Since density defines how atoms are closely packed in a given structure, its enhancement validated the increase in the tight atomic arrangement and the rigidness of the glasses. The molar volume trend, on the other hand, contrasted that of density; the value recorded an initial decrease in response to varying the dopant's contents and then increased, reaching a maximum value of 32.1 cm^3 mol^{-1} corresponding to BSm5glass sample. The decreasing trend of the molar volume may be ascribed to the rearrangement of the lattice structure, thereby reducing the glass porosity [47]. Upon addition to the borate glass matrix, Sm^{3+} creates a local structural distortion by creating non-bridging oxygen and causes the borate network to become relaxed and less ordered. As a result of this structural distortion, there is a reduction in both the average bond lengths and bond angles present in the glass, consequently leading to a decrease in the molar volume of the glass.

3.2.5. Bandgap energy, refractive index, and molar refractivity

The indirect Bandgap energy, refractive index, and molar refractivity of the glass samples are furnished in Table 4. The band gap energies were determined from the absorption spectra using the linear fitting method of Tauc plot in accordance with the methodology described in references [48,49]. Fig. 6 display the Tauc's plot of the glass samples. The refractive indices were derived from the Bandgap energies, and the molar refractivities were estimated afterwards. A slight increase in the Bandgap energy was initially recorded with the increase in Sm^{3+} contents in analogy with the report of Eraiah relating to lead-tellurite glass doped with Sm^{3+} [48] and in contrast with the findings of Okasha et al. in the case of Sm^{3+} activated zinc-lead-phosphate glasses [50]. The observed increase in the Bandgap energy results from the enhancements in the bonding defect and non-bridging oxygen. Therefore, the optical

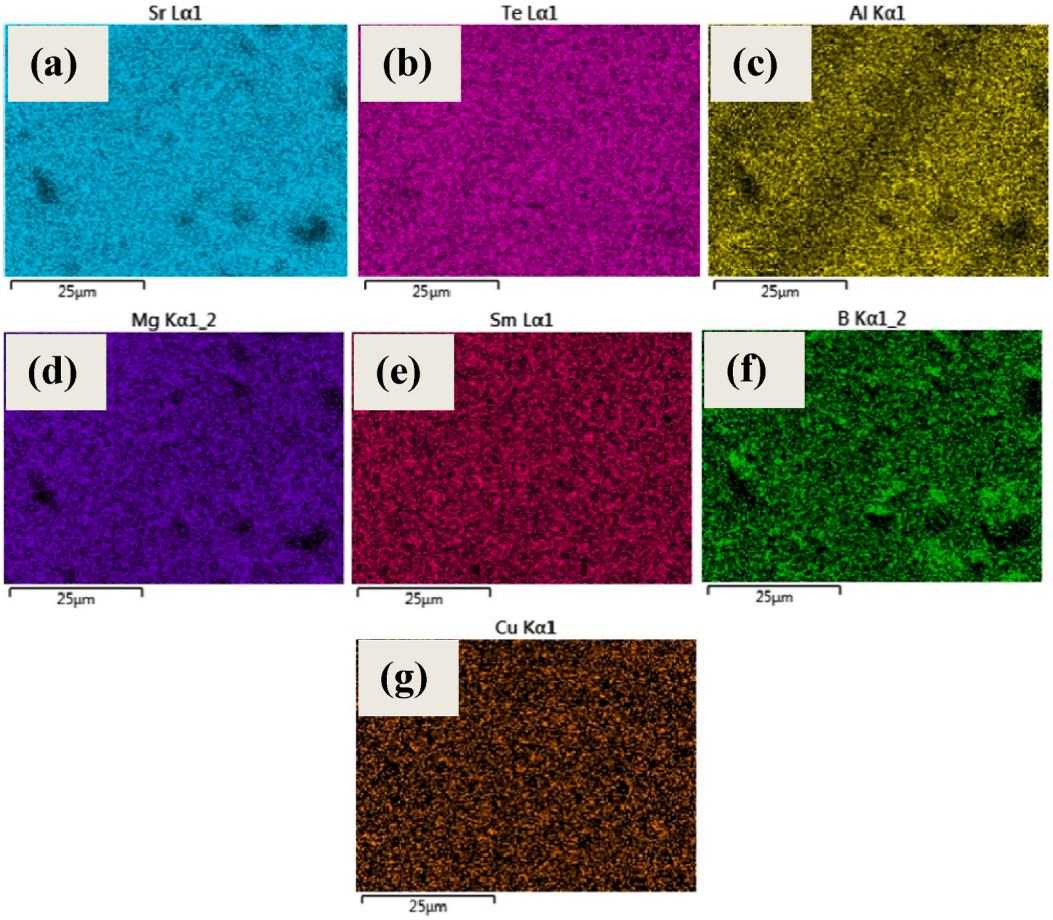

Fig. 4. EDX maps of BCSm3 glass showing the existence of: (a) Strontium (b) Tellurium (c) Aluminium (d) Magnesium (e) Samarium (f) Boron and (g) Copper.

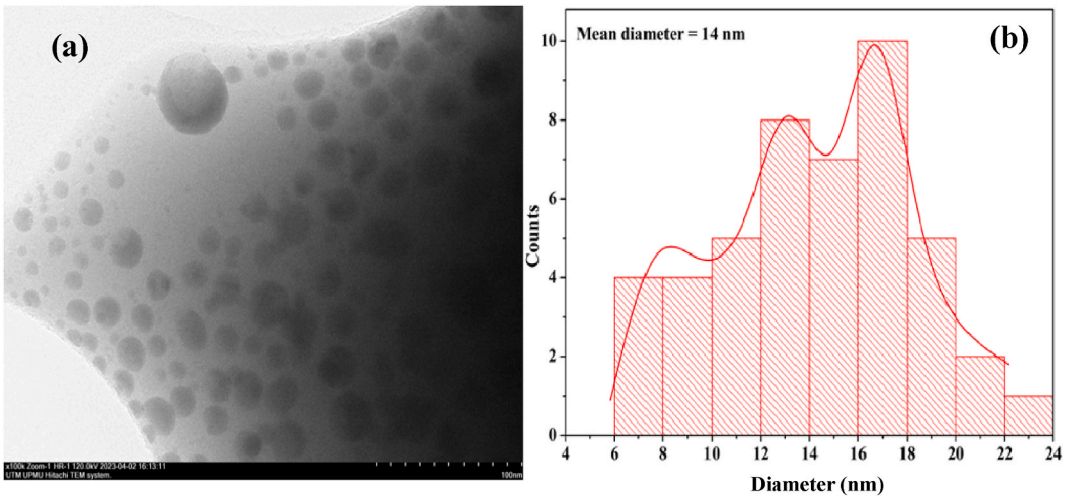

Fig. 5. (a) HRTEM image of BCSm3 glass and (b) nanoparticles size distribution.

Table 4
Physical and optical properties of the synthesized glasses.

Glass code	Physical parameter			Optical parameter		
	Density (±0.01 g cm^{-3})	Molar volume (cm^3 mol^{-1})	Ionic concentration (× 10^{22} ions cm^{-3})	Bandgap (±0.2 eV)	Refractive Index	Molar refractivity (cm^3 mol^{-1})
BSm1	2.799	31.408	0.957	3.554	2.179	17.29
BSm2	2.820	31.271	1.348	3.547	2.180	18.01
BSm3	2.841	31.346	1.911	3.562	2.179	18.04
BSm4	2.832	31.654	2.283	3.533	2.181	18.32
BSm5	2.820	32.064	2.817	3.541	2.180	18.46
BCSm3	2.845	31.346	1.921	3.221	2.213	17.65

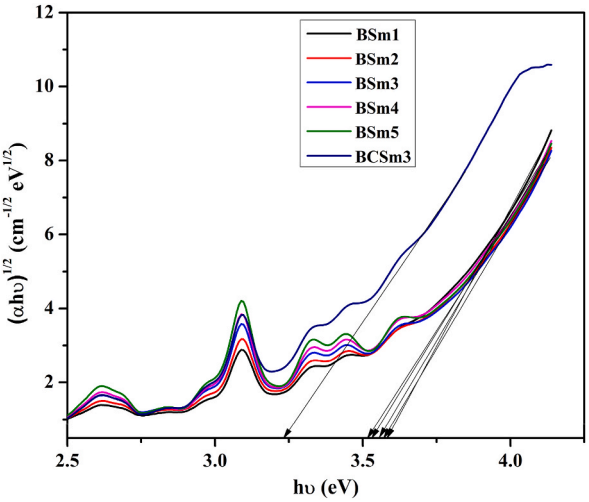

Fig. 6. Tauc plot of the developed glasses.

characteristics of the glass, including refractive index, transparency, and molar refractivity, were significantly improved. Whilst the refractive index enhancement improves the optical transparency of the glasses, the enhancement in the molar refractivity is known to be beneficial for optical amplification, fiber optics, and laser technology.

3.3. UV–Vis–NIR absorption spectra

UV–Vis–NIR absorption spectroscopy was utilized to investigate the electronic energy level structure, optical transition properties, and overall optical characteristics of the synthesized glasses. The obtained insights can be valuable for optimizing the performance of

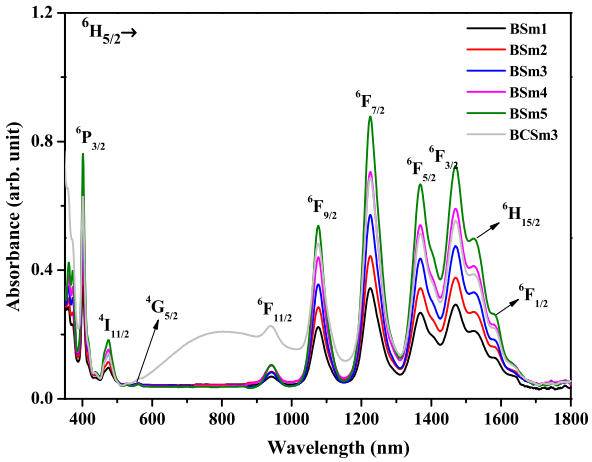

Fig. 7. Absorption spectra of the fabricated BSm and BCSm3 glasses.

these glasses for various applications. Fig. 7 displays the obtained absorption spectra matching the Sm^{3+} transition from and to various energy levels. The identification of the ten (10) prominent f-f transition bands was established using the information provided in references [51,52]. It was noticed that the absorbance of the glass samples increased progressively with increasing Sm^{3+} concentration; thus, BSm1 showed the least absorbance, whereas BSm5 yielded the highest absorbance. Close observation was reported by Mahmud et al. in the case of Sm^{3+} doped lead borosilicate glasses [53]. Moreover, the band shapes and positions were not affected by varying the Sm_2O_3 contents. Furthermore, the observed transitions from the ground state $^6H_{5/2}$ to the manifold ^6F and ^6H levels are more intense in comparison with ^4F and ^4G transitions; Zalamin et al. argued that the high intensity is due to the spin-allowed selection rule ($\Delta S = 0$) [54]. However, the introduction of copper oxide nanoparticles reasonably enhanced the absorbance of the glass samples, as evidenced by the absorption spectra. The enhancement covered the visible to infrared region but is more prominent in the visible region. The mechanism for the absorption amplification by the copper oxide nanoparticles may be explained by the effects of the strong absorption of octahedrally coordinated Cu^{2+} [55]. Apparently, Ouis et al. holds that copper oxide nanoparticles produce rich absorption as a result of the splitting of Cu^{2+}'s d energy level into two ground states ($2E_g$), which in turn generate ternary excited levels ($2T_g$), which are then transformed into overlapping levels of $2B_{1g}$, $2A_{1g}$, $2B_{2g}$, and $2E_g$ Ref. [55]. Another possible absorption enhancement mechanism is the combined effects of the surface plasmon resonance and energy transfer processes.

3.4. Oscillator strengths and judd-ofelt analysis

The probability of the occurrence of a given transition is checked using the oscillator strengths. The oscillator strengths of the Sm^{3+} transitions in the current glasses, as developed using the theoretical formulations of Judd and Ofelt (JO) [56–58], were presented in Table 5. As evidenced from the Table, the oscillator strength of $^6H_{5/2} \rightarrow {}^6F_{7/2}$ Sm^{3+} transition is most substantial in all the developed glass samples (Fig. 7). Hence, this transition was picked as a reference for discussion. The dominant nature in the oscillator strengths of the $^6H_{5/2} \rightarrow {}^6F_{7/2}Sm^{3+}$ transition is possible due to the allowed spin selection rules [53]. Moreover, it was observed that the oscillator strength of the transition decreased continuously with the rise in the Sm_2O_3 contents up to 1.0 mol%. However, a reversed trend was witnessed as the Sm_2O_3 content increased beyond 1.0 mol%. The observed decrease in the oscillator strengths indicates the transformation of the Sm^{3+}-Ligand bond from covalent to ionic [59]. Furthermore, the incorporation of copper oxide nanoparticles was found to instigate the decrease in the oscillator strength from 1.777×10^{-6} to 1.773×10^{-6}; hence, copper oxide nanoparticles in the current glass host attenuated the covalency of the Sm^{3+}-ligand bond.

The JO intensity parameters obtained from the evaluated oscillator strengths are presented in Table 6. Except for the copper oxide nanoparticles embedded glass sample (BCSm3), the intensity parameters of all the glasses obeyed the pattern $\Omega_6>\Omega_4>\Omega_2$; a similar trend was reported by Mohammed et al. regarding Sm^{3+} activated calcium sulfate phosphate glasses [60]. The incorporation of copper oxide nanoparticles ensured the change in the pattern to $\Omega_4>\Omega_6>\Omega_2$. The trend modification was linked to changes in the local environment around the sm^{3+}. While the covalency of the Sm–O bond was attenuated (due to a reduction in Ω_2), the rigidity of the glass sample was increased considerably (enhancement of Ω_4 and Ω_6). This stimulated the spectroscopic quality factor enhancement and the subsequent trend modification. Since the values of Ω_4 and Ω_6 define the rigidity of the glass samples, the higher values obtained herein in comparison with Ω_2 values attested to the rigidity of the glass samples [53]; the density pattern of the glasses confirms this. On the other hand, the lower values of Ω_2 validated the low covalency and high symmetry of the Sm ions environment in the glass systems [61]. It was observed that the increase in the Sm_2O_3 contents up to 1.0 mol% ensured the decrease in the Ω_2 value from 0.294×10^{-20} to 0.265×10^{-20} cm^2; thus, it was concluded that the covalency of the Sm^{3+} bond is weakened with increasing Sm^{3+} concentration. Ω_4 and Ω_6 exhibited a similar trend; however, their combined effect improved the spectroscopic quality factor from 0.921 to 1.081, a value higher than the reported value of 0.591 for Sm^{3+} doped phosphate-based glasses [60]. The achieved spectroscopic quality factor is fit for lasing application.

3.5. Photoluminescence spectra and radiative properties

The emission spectral acquisition for the current glass samples was performed using 401 nm excitation wavelengths. This

Table 5
Measured (f_e) and calculated (f_c) oscillator strengths of the glass samples.

Transition $^6H_{15/2} \rightarrow$	Oscillator strengths ($\times 10^{-6}$)											
	BSm1		BSm2		BSm3		BSm4		BSm5		BCSm3	
	f_e	f_c	f_e	f_c	f_e	f_c	f_e	f_c	f_e	f_c	f_e	f_c
$^6P_{3/2}$	0.358	1.404	0.357	1.406	0.331	1.354	0.336	1.358	0.309	1.388	0.315	1.509
$^4I_{11/2}$	0.134	0.083	0.125	0.080	0.129	0.077	0.128	0.079	0.146	0.080	0.154	0.076
$^6F_{11/2}$	0.196	0.201	0.102	0.194	0.107	0.187	0.116	0.192	0.106	0.194	0.082	0.183
$^6F_{9/2}$	1.000	1.219	0.949	1.178	0.921	1.133	0.946	1.165	0.952	1.175	0.856	1.119
$^6F_{7/2}$	1.830	1.671	1.789	1.625	1.715	1.564	1.755	1.600	1.777	1.619	1.773	1.585
$^6F_{5/2}$	0.803	0.717	0.804	0.718	0.783	0.691	0.789	0.699	0.822	0.712	0.896	0.780
$^6F_{3/2}$	0.468	0.397	0.458	0.393	0.433	0.377	0.458	0.403	0.438	0.404	0.503	0.464
$^6H_{15/2}$	0.139	0.010	0.111	0.001	0.117	0.095	0.107	0.010	0.176	0.010	0.145	0.009
$^6F_{1/2}$	0.043	0.107	0.042	0.101	0.043	0.096	0.073	0.126	0.078	0.119	0.114	0.160
δ_{rms} ($\times 10^{-6}$)		0.449		0.45		0.438		0.437		0.464		0.221

Table 6
Judd-Ofelt intensity parameters ($\times 10^{-20}$ cm^2) of the studied glasses.

Glass Name	Ω_2	Ω_4	Ω_6	Pattern	$\chi = \Omega_4/\Omega_6$	Reference
BSm1	0.294	1.131	1.228	$\Omega_6>\Omega_4>\Omega_2$	0.921	This work
BSm2	0.279	1.131	1.184	$\Omega_6>\Omega_4>\Omega_2$	0.956	This work
BSm3	0.265	1.089	1.137	$\Omega_6>\Omega_4>\Omega_2$	0.958	This work
BSm4	0.348	1.091	1.169	$\Omega_6>\Omega_4>\Omega_2$	0.933	This work
BSm5	0.329	1.114	1.179	$\Omega_6>\Omega_4>\Omega_2$	0.945	This work
BCSm3	0.153	0.532	0.522	$\Omega_4>\Omega_6>\Omega_2$	1.018	This work
CSP; Sm	0.152	6.338	10.724	$\Omega_6>\Omega_4>\Omega_2$	0.591	[60]
Sm1	5.145	7.866	2.757	$\Omega_4>\Omega_2>\Omega_6$	15.42	[61]
PNZSm0.5	4.460	6.790	10.910	$\Omega_6>\Omega_4>\Omega_2$	0.620	[62]
Li_2O–PbO–H_3BO_3	0.845	3.513	3.540	$\Omega_6>\Omega_4>\Omega_2$	0.992	[63]
5NdCuO	3.89	5.75	9.93	$\Omega_6>\Omega_4>\Omega_2$	0.579	[64]

wavelength matched with the most intense absorption transition of Sm^{3+} at the absorption edge. Fig. 8 provides a clear representation of the emission spectra observed in the glasses. For all the glass samples, the spectral profile exhibited four characteristics bands of Sm^{3+} emission; these bands are centered at 561, 598, 645, and 705 nm, tallying with $^4G_{5/2} \rightarrow {}^6H_{5/2}$, $^4G_{5/2} \rightarrow {}^6H_{7/2}$, $^4G_{5/2} \rightarrow {}^6H_{9/2}$, and $^4G_{5/2} \rightarrow {}^6H_{11/2}$ transitions, respectively. The nature and details of the observed emission bands were reported by Kolavekar et al. [65]. Furthermore, while the spectral shapes and positions were not altered by varying the Sm content, the emission bands' intensity was increased by increasing the Sm_2O_3 contents up to 1.0 mol%, beyond which the intensity quenches. Hence, the BSm3 glass sample was chosen as the optimum concentration. Krishna et al. reported analogous observations relating to Sm^{3+} doped oxy-fluoro-borotellurite glass system [66]. They also attributed the luminescence quenching effect at higher concentrations to the cross-relaxation channels arising from resonant and non-radiative energy transfer processes. Among all the emission bands, the reddish-orange $^4G_{5/2} \rightarrow {}^6H_{7/2}$ is the most intense and thus was chosen for the comparison of the intensity magnitude as a function of Sm_2O_3 contents, as displayed in Fig. 9. In addition, the exceptional intensity of this transition makes it ideal for diverse applications such as color displays, high-density optical storage devices, and also in medical diagnostics [66]. From Fig. 8, one can observe the effects of incorporating copper oxide nanoparticles into the glass matrix. Although the shape and position of the bands remained unaltered, there was a slight reduction in intensity. The attenuation of the emission intensity with the introduction of CuO was attributed to either luminescence quenching effect due to reduction in the Sm^{3+} interionic distances, energy transfer from Sm^{3+} to Cu^{2+}, or Both [67]. In the former case, the introduction of CuONps results in the congestion of ions in the glass samples, this reduced the Sm^{3+}-Sm^{3+} distances and favours luminescence quenching effect leading to the observed decrease in the emission intensity. In the latter case, instead of the normal radiative processes, energy is transferred from Sm^{3+} to Cu^{2+} (mediated by electric dipole-dipole interactions) and this result in the decrease of the emission intensity [68]. During the heating process, copper oxide nanoparticles were oxidized to Cu^{2+},and since considerable spectral overlap between their absorption in the visible region and the emission of Sm^{3+}, the possibility for the occurrence of resonant Sm^{3+}-Cu^{2+} energy transfer is very high and the result is the decrease in the Sm^{3+} emission intensity [69]. The partial energy level diagram of Sm^{3+} ions in the current glass system is shown in Fig. 10.

The radiative properties of the dominant emission transition ($^4G_{5/2} \rightarrow {}^6H_{7/2}$) evaluated using the JO model are presented in Table 7. For all the developed glasses, the branching ratio (β_R) value is greater than 80%, and an emission cross-section (δ_E) as high as 135.82×10^{-23} cm^2 was realized. These values are higher than the reported values of 55% and 88×10^{-25} cm^2 s^{-1}, respectively, in the case of the Sm^{3+} activated metal fluorophosphate glass system [70]. The revealed higher β_R and δ_E values indicate the ability of the glasses to favour stimulated emission, an essential property required for lasing application [71]. Furthermore, the large values of radiative lifetime τ_R (>3.5 ms) and the optical gain $\delta_E\times\tau_R$ ($>46\times10^{-25}$ cm^2 s^{-1}) attested to the suitability of $^4G_{5/2} \rightarrow {}^6H_{7/2}$ transition for optical lasing and amplification. While the branching ratio (β_R) increased from 81.9 to 82.589% with increasing Sm_2O_3 contents up to 1.0 mol%, the emission cross-section (δ_E) value attenuated from 135.82×10^{-23} cm^2 to 130.74×10^{-23} cm^2 in response. τ_R and $\delta_E\times\tau_R$ exhibited similar pattern as well. It is important to note that while the incorporation of copper oxide nanoparticles slightly attenuated the branching ratio and radiative lifetime, it stimulated the enhancement of δ_E and the optical gain by almost 1.1-fold. The recorded enhancements confirmed the copper oxide nanoparticles' role in improving the glass systems' lasing and optical amplification potentials [72].

Based on the disclosure of the radiative parameters, the current glass systems if selected will be beneficial for several practical applications such as laser, optical fiber, photonics, and display. For example, the higher $\beta_R > 80\%$, and $\tau_R > 3.5$ ms guarantees the possibility of large stimulated emission probability, a key aspect for the lasing material. Furthermore, the large value of δ_E up to 135.82×10^{-23} cm^2 and $\delta_E\times\tau_R > 46\times10^{-25}$ cm^2 s^{-1} favours optical amplification.

3.6. CIE 1931 chromaticity analysis

The CIE 1931 chromaticity diagram for the current BSm glasses, as evaluated from the emission spectra at 401 nm excitation wavelengths is shown in Fig. 11. The CIE chromaticity has become a noble platform for examining the emission color of rare earth ions activated glasses sensible to human eyes. Table 8 presents the color coordinates for the glasses under the current study. For all the synthesized glasses, the chromaticity coordinates fall within the yellowish-orange to reddish-orange region in resonance with the reports of Shoaib et al. relating to Sm^{3+} activated phosphate based glasses [76], Yuliantini et al. in Sm^{3+} doped zinc-alumino-borate

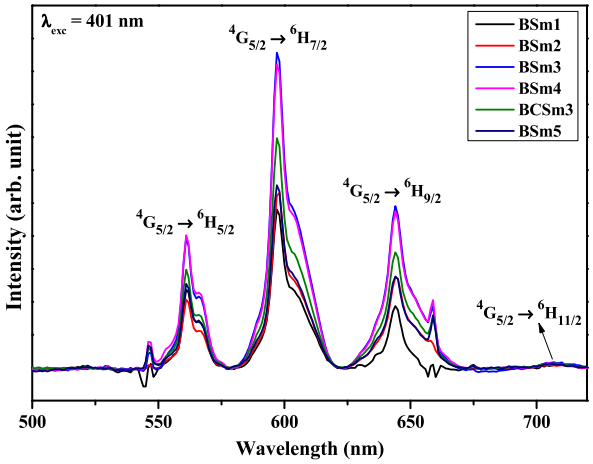

Fig. 8. Photoluminescence emission spectra of the studied glasses.

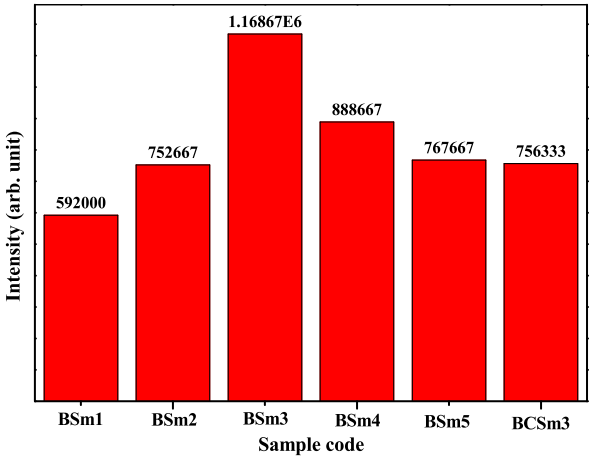

Fig. 9. Intensity of $^4G_{5/2} \rightarrow {}^6H_{7/2}$ emission band in the fabricated glasses.

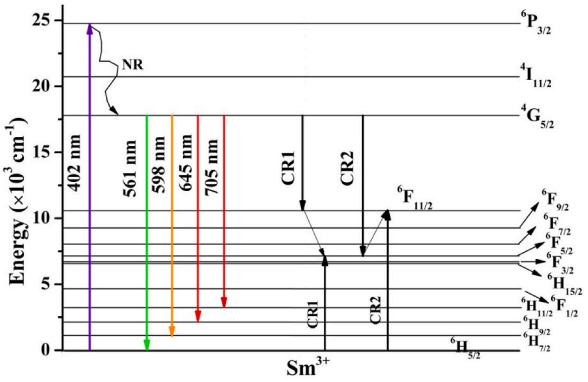

Fig. 10. Partial energy level diagram of Sm^{3+} in BSm glasses.

based glasses [77], and Rajesh et al. in Sm^{3+} activated flouroborosilicate glasses [78]. It was observed that the introduction of copper oxide nanoparticles shifted the chromaticity coordinates to the extreme end of the reddish-orange zone; structural readjustments, symmetry change, and covalent modification within the glass samples were responsible for the observed color tunability [79]. The implication of the perceived color purity and the shift in the chromaticity coordinates to the reddish-orange zone indicated that the

Table 7
Radiative properties of Sm^{3+} transition in the studied glasses.

Glass Sample	β_R (%)	δ_E ($\times 10^{-23}$ cm^2)	τ_R (ms)	$\delta_E \times \tau_R$ ($\times 10^{-25}$ cm^2 s^{-1})	Reference
BSm1	81.900	135.820	3.618	49.134	This work
BSm2	82.223	129.680	3.633	47.117	This work
BSm3	82.589	130.740	3.680	48.107	This work
BSm4	81.939	127.154	3.638	46.259	This work
BSm5	81.858	127.381	3.624	46.162	This work
BCSm3	80.515	143.279	3.557	50.970	This work
PZSMS1.0	51.562	95.762	0.673	64.448	[62]
MgSm5	55.000	88.000	–	78.000	[70]
BCSSm	56.000	115.000	.	.	[73]
PKAZFSm	51.000	115.000	–	–	[74]
LBZnFSm10	63.000	157.630	1.904	30.013	[75]

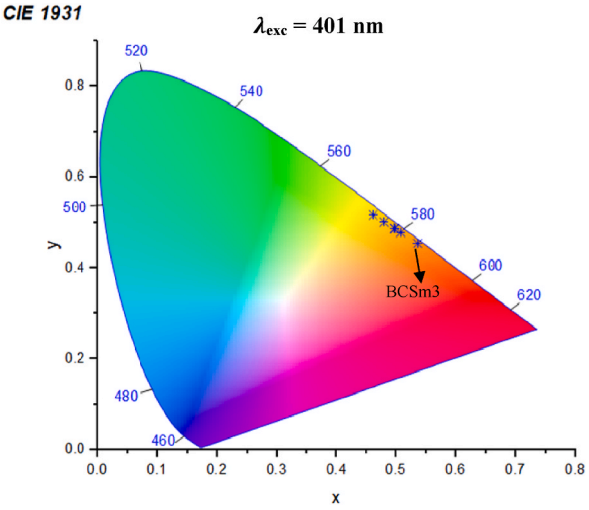

Fig. 11. CIE 1931 chromaticity diagram of the developed glasses at 401 nm excitation wavelength.

Table 8
The CIE chromaticity coordinates of the prepared glasses.

Glass System	CIE coordinates	
	x	y
BSm1	0.460655	0.516900
BSm2	0.479732	0.501121
BSm3	0.496440	0.487332
BSm4	0.507073	0.478347
BCSm3	0.535257	0.454147

optical properties of the glass are tunable. In addition, Sm^{3+} activation can introduce energy levels within the glass matrix, leading to the optical absorption and emission of specific wavelengths. This can be utilized in various optical devices, such as lasers, and light-emitting diodes, where specific colors or wavelengths are required. On top, the shift in chromaticity coordinates can serve as a useful tool for characterizing the developed glass system. By analyzing the change in color, researchers and scientists can gain insights into the dopant concentration, energy levels, and electronic transitions occurring within the glass structure. The CIE pattern exhibited by the studied glasses indicates their suitability for reddish-orange lasing applications.

3.7. Thermal-physical-optical correlations

The thermal properties of the glass systems correlate well with the corresponding structural and optical properties. For example, as the thermal stability factor of the BSm1 glass sample increased from 118° to 120° and then 122° due to the increment in the Sm_2O_3 content from 0.5 to 0.7 and 1.0 mol%, respectively, the density responded in the same manner, increasing from 2.799 to 2.82 and then 2.841 g cm^{-3}, respectively. The refractive index also increased from 2.179 to 2.18 and then 2.179, respectively. This observation

indicates the correlation between the glasses' thermal, physical, and optical properties. The radiative properties also correlate with the other properties in the same manner wherein the τ_R increased from 3.618 to 3.633 and then 3.68 ms, respectively. Similarly, the β_R value was enhanced from 81.9 to 81.22 and then 82.589%, respectively. The observed correlation is a consequence of the interconnected nature of the glass structure and its properties. It is crucial for fundamental understanding, performance optimization, and application development in various fields, such as lasing and optical fiber amplification.

4. Conclusion

The influence of Sm^{3+} doping at various level and copper oxide nanoparticles (at optimum content) embedment on the thermal, structural, physical, and luminescence properties of strontium-telluro-alumino-magnesium-borate glass hosts were evaluated. Thermally stable and optically transparent glasses were achieved wherein their stability factor was increased with the increase of Sm_2O_3 doping levels. The spectroscopic attributes of the glasses such as the branching ratio and stimulated emission cross-section of the glasses responded to the Sm^{3+} concentration changing accordingly. While branching ratio above 80% and stimulated emission cross-section up to 135.82×10^{-23} cm^2 were achieved through Sm^{3+} concentration tuning, the radiative lifetime and optical gain were enhanced to 3.68 ms and 50.97×10^{-25} $cm^2\,s^{-1}$ respectively. Thus, it was demonstrated that the overall attributes of these glasses can be customized by Sm_2O_3 and copper oxide nanoparticles incorporation. The observed improvement in the optical absorption, emission and radiative properties of the glasses was ascribed to the glass network structure modification as confirmed from FTIR, XRD, and HRTEM data analyses. The shift of the chromaticity coordinates from yellowish-orange to reddish-orange zone as a function of Sm_2O_3 was a strong indicator of visible luminescence tuning. The proposed glass compositions may be potential for various photonic applications.

Author contribution statement

Ibrahim Abdullahi: Conceived and designed the experiments; Performed the experiments; Analyzed and interpreted the data; Wrote the paper.

Suhairul Hashim: Sib Krishna Ghoshal: Analyzed and interpreted the data; Contributed reagents, materials, analysis tools or data; Wrote the paper.

M. I. Sayyed: Analyzed and interpreted the data.

Data availability statement

The authors do not have permission to share data.

Declaration of competing interest

The authors declare that they have no known competing financial interests or personal relationships that could have appeared to influence the work reported in this paper.

Acknowledgments

We acknowledged the post-doctoral fellowship assistance from Universiti Teknologi Malaysia (UTM) under the Professional Development Research University (R.J130000.7113.06E41) initiatives. MI Sayyed and S. Hashim gratefully acknowledge Universiti Teknologi Malaysia for supporting their Prominent Visiting Researcher Scheme (RJ3000.7113.3F000) through the Department of Deputy Vice-Chancellor (Research and Innovation).

References

[1] S.M. Bezerra, V. Levchenko, F. Piccinelli, M. Bettinelli, R.L. Longo, O.L. Malta, R. Reisfeld, Amplification of light emission of lanthanide complexes by copper and copper oxide nanoparticles, J. Lumin. 251 (2022), 119217, https://doi.org/10.1016/j.jlumin.2022.119217.

[2] H. Lin, H. Yang, L. Zhou, J. He, B. Liu, N. Li, C. Li, S. Li, W. Yang, X. Jiang, H. Liu, F. Zeng, Z. Su, Research on the physical and optical properties of Dy^{3+} doped 30 mol % verdet constant, J. Phys. Chem. Solids. 166 (2022), 110682, https://doi.org/10.1016/j.jpcs.2022.110682.

[3] K. Keshavamurthy, G. Jagannath, D. Abdullah, A. Aljawhara, Silver nanoparticles amplified visible and infrared photoluminescence features of Er^{3+} ions activated in borate glasses, Plasmonics (2023) 175–182, https://doi.org/10.1007/s11468-022-01736-2.

[4] M. Milanova, L. Aleksandrov, A. Yordanova, R. Iordanova, N.S. Tagiara, A. Herrmann, G. Gao, L. Wondraczek, E.I. Kamitsos, Structural and luminescence behavior of Eu^{3+} ions in ZnO-B2O3-WO3 glasses, J. Non-Cryst. Solids 600 (2023), 122006, https://doi.org/10.1016/j.jnoncrysol.2022.122006.

[5] V.R.L. Murty, M. Venkateswarlu, K. Swapna, S. Mahamuda, P.R. Rani, A.S. Rao, Physical and spectroscopic studies of Sm^{3+} ions doped Alumino Tungsten Borate glasses for photonic applications, Radiat. Phys. Chem. 190 (2022), 109806, https://doi.org/10.1016/J.RADPHYSCHEM.2021.109806.

[6] A. Dehelean, S. Rada, J. Zhang, Determination of the lead environment in samarium – lead oxide-borate glasses and vitroceramics using XANES and EXAFS studies, Radiat. Phys. Chem. 174 (2020), 108927.

[7] A. Herrmann, M. Zekri, R. Maalej, C. Rüssel, The effect of glass structure on the luminescence spectra of Sm^{3+}-doped aluminosilicate glasses, Materials 16 (2023), https://doi.org/10.3390/ma16020564.

[8] H. Lin, S. Tanabe, L. Lin, Y.Y. Hou, K. Liu, D.L. Yang, T.C. Ma, J.Y. Yu, E.Y.B. Pun, Near-infrared emissions with widely different widths in two kinds of Er^{3+}-doped oxide glasses with high refractive indices and low phonon energies, J. Lumin. 124 (2007) 167–172, https://doi.org/10.1016/j.jlumin.2006.02.019.

[9] X. Zhang, W. Xu, J. Zhang, P. Huang, X. Qi, High-entropy oxide glasses TiO_2-$Ta_2O_5Nb_2O_5$-WO_3−MOx (M=La/Sm/Eu/Tb/Dy) with high refractive index, J. Non-Cryst. Solids 597 (2022), 121862, https://doi.org/10.1016/j.jnoncrysol.2022.121862.

[10] X. Wang, M. Zhang, K. Chen, W. Deng, X. Liu, F. Wu, Y. Zhang, Y. Zhang, Optical, mechanical and thermal properties in HfO_2-doped TiO_2-$Lao_{3/2}$ glasses fabricated by aerodynamic levitation, Mater. Res. Bull. 158 (2023), 112079, https://doi.org/10.1016/j.materresbull.2022.112079.

[11] S. Singla, V. Gopal, N. Mahendru, S.S. Prabhu, M. Falconieri, G. Sharma, High refractive index gold nanoparticle doped Bi2O3-B_2O_3 glasses for THz frequencies, Opt. Mater. 72 (2017) 91–97, https://doi.org/10.1016/j.optmat.2017.05.043.

[12] G. Swapna, Upender, M. Prasad, Raman, FTIR, thermal and optical properties of TeO_2-Nb_2O_5-B_2O_3-V_2O_5 quaternary glass system, J. Taibah Univ. Sci. 11 (2017) 583–592, https://doi.org/10.1016/J.JTUSCI.2016.02.008.

[13] R. Miedzinski, I. Fuks-Janczarek, L.R.P. Kassab, F.A. Bomfim, Second and third-order nonlinear optical properties of Er^{3+}/Yb^{3+} doped PbO-GeO_2-Ga_2O_3 glasses with Au nanoparticles, Mater. Res. Bull. 95 (2017) 339–348, https://doi.org/10.1016/j.materresbull.2017.08.009.

[14] C.S. Sarumaha, J. Rajagukguk, N. Chanthima, P. Kidkhunthod, N. Chanlek, P. Kantuptim, T. Yanagida, H.J. Kim, J. Kaewkhao, Luminescence characteristics of Ce^{3+} doped multicomponent lithium fluorophosphate glasses, Radiat. Phys. Chem. 207 (2023), 110814, https://doi.org/10.1016/j.radphyschem.2023.110814.

[15] S.B. Kolavekar, G.B. Hiremath, P.N. Patil, N.M. Badiger, N.H. Ayachit, Investigation of gamma-ray shielding parameters of bismuth phospho-tellurite glasses doped with varying Sm_2O_3, Heliyon 8 (2022), e11788, https://doi.org/10.1016/j.heliyon.2022.e11788.

[16] I. Khan, M. Shoaib, N. Srisittipokakun, I. Ullah, A. Ahad, S. Kothan, G. Rooh, J. Kaewkhao, Spectroscopic investigation of Sm_2O_3-activated barium calcium strontium borate glasses for laser and display-devices applications, Optik 265 (2022), 169439, https://doi.org/10.1016/J.IJLEO.2022.169439.

[17] S. Kumari, Anu, A. Prasad, P. Rohilla, A.S. Rao, Prospective applications of thermally stable Dy^{3+} doped potassium zinc strontium borate (KZSB) glasses in w-LEDs, J. Mater. Sci. Mater. Electron. 34 (2023) 1–17, https://doi.org/10.1007/s10854-023-10272-6.

[18] B. Narsimha, K. Chandra Sekhar, M. Shareefuddin, Ramadevudu Gokarakonda, Copper doped strontium Indium-borate glasses: FTIR, Raman, EPR, optical and structural studies, Mater. Today Proc. (2023) 2–9, https://doi.org/10.1016/j.matpr.2023.05.185.

[19] A.H. Hammad, A.M. Abdelghany, H.A. Elbatal, The influence of titanium ions on crystallization, morphological, and structural properties of strontium borate glass, J. Non-Cryst. Solids 450 (2016) 66–74, https://doi.org/10.1016/j.jnoncrysol.2016.07.033.

[20] A. S, K. Marimuthu, Concentration effect of Sm^{3+} ions in B_2O_3–PbO–PbF_2–Bi_2O_3–ZnO glasses–Structural and luminescence investigations, J. Alloys Compd. 565 (2013) 104–114.

[21] A. Anu, Ravina Kumar, N. Deopa, A.S. Rao, Efficient tunable photoluminescence of Dy^{3+}/Eu^{3+} co-doped OFSZBS glasses for warm white LEDs, J. Non-Cryst. Solids 616 (2023), 122421, https://doi.org/10.1016/j.jnoncrysol.2023.122421.

[22] M.A. Marzouk, A.M. Fayad, F.H. ElBatal, Crystallization effects on the photoluminescence efficiency of SrO-B_2O_3 glass activated by W^{6+}, Eu^{3+}, Dy^{3+} or Pr^{3+} ions, Spectrochim, Acta-Part A Mol. Biomol. Spectrosc. 274 (2022), 121079, https://doi.org/10.1016/j.saa.2022.121079.

[23] E.M. Bouabdalli, M. El Jouad, N. Gaumer, M. Siniti, S. Touhtouh, A. Hajjaji, Structural, physical, thermal and optical spectroscopy studies of the europium doped strontium phosphate glasses, Inorg. Chem. Commun. 151 (2023), 110563, https://doi.org/10.1016/j.inoche.2023.110563.

[24] N.S. Sabri, M.K. Talari, Optical properties of xSrO-(90-x)B_2O_3-2CeO_2-8Al_2O_3 glasses, Mater. Today Proc. 66 (2022) 4045–4050, https://doi.org/10.1016/j.matpr.2022.05.534.

[25] A.U. Ahmad, S. Hashim, S.K. Ghoshal, Physical , thermal and absorption traits of lithium strontium zinc borate glasses : sensitiveness on Dy^{3+} doping, J. Alloys Compd. 844 (2020), 156176, https://doi.org/10.1016/j.jallcom.2020.156176.

[26] R. Stefan, L.C. Bolundut, L. Pop, G. Borodi, E. Culea, P. Pascuta, Copper nanoparticles enhanced luminescence of Eu^{3+} doped lead tellurite glass ceramics, J. Non-Cryst. Solids 505 (2019) 9–17, https://doi.org/10.1016/j.jnoncrysol.2018.10.031.

[27] K.B. Manjunatha, R.S. Bhat, A. Shashidhara, H.S.A. Kumar, S. Nagashree, Antimicrobial and nonlinear optical studies of copper oxide nanoparticles, J. Electron. Mater. 50 (2021) 3415–3421, https://doi.org/10.1007/S11664-021-08838-3/FIGURES/7.

[28] I. Abdullahi, S. Hashim, M.I. Sayyed, S.K. Ghoshal, Intense up-conversion luminescence from Dy^{3+}-doped multi-component telluroborate glass matrix: role of CuO nanoparticles embedment, Heliyon 9 (2023), e15906, https://doi.org/10.1016/j.heliyon.2023.e15906.

[29] S. Norul, F. Zalamin, M. Hafiz, M. Zaid, K. Amin, M. Khalis, A. Karim, N. Afiqah, M. Yamin, N. Atikah, N. Ismail, Comprehensive study on optical and luminescence properties of Sm^{3+} doped magnesium borotellurite glasses, J. Phys. Chem. Solids. 163 (2022), 110563, https://doi.org/10.1016/j.jpcs.2021.110563.

[30] G. El Damrawi, R. Mohammed Ramadan, M. El Baiomy, Structural role of strontium oxide in modified silicate glasses, Silicon 14 (2022) 4879–4885, https://doi.org/10.1007/s12633-021-01226-w. Published.

[31] N.E. Shchegoleva, L.A. Orlova, A.S. Chainikova, D.V. Grashchenkov, Effect of the additives B_2O_3 and P_2O_5 on silicate and glass-formation processes in making strontium aluminosilicate glasses, Glas. Ceram. (English Transl. Steklo i Keramika). 78 (2021) 97–103, https://doi.org/10.1007/s10717-021-00355-3.

[32] N. Liyana, A. Rodin, M.R. Sahar, Erbium doped sodium magnesium boro-tellurite glass : stability and Judd- Ofelt analysis, Mater. Chem. Phys. 216 (2018) 177–185, https://doi.org/10.1016/j.matchemphys.2018.06.006.

[33] I. Abdullahi, S. Hashim, S.K. Ghoshal, M.I. Sayyed, H.A.A. Thabit, N.N. Yusof, Enhanced up- and down-conversion luminescence from Dy^{3+}-Sm^{3+} co-doped B_2O_3-$SrCO_3$-TeO_2-Al_2O_3-MgO glass hosts: effects of CuO nanoparticles embedment, Phys. Scr. 98 (2023) 065511. http://iopscience.iop.org/article/10.1088/1402-4896/acd152.

[34] M.R. Sahar, E. Jaafar, S.K. Goshal, Luminescence spectra of erbium doped zinc tellurite glass embedded with gold nanoparticles, Adv. Mater. Res. 895 (2014) 231–235. https://dx.doi.org/10.4028/www.scientific.net/AMR.895.231.

[35] D. Vijayasri, K.S. Rudramamba, T. Srikanth, N.M. Reddy, M. Nakka, S. Pratyusha, M.R. Reddy, Spectroscopic features of Tb^{3+} doped strontium zinc borate glasses for green laser applications, J. Mol. Struct. 1274 (2023), 134514, https://doi.org/10.1016/j.molstruc.2022.134514.

[36] P. Li, X. Zhang, J. Zhang, X. Qi, X. Liu, Investigations of thermal stability and spectroscopic features of Sm^{3+} doped strontium aluminate glasses, Coatings 12 (2022), https://doi.org/10.3390/coatings12010003.

[37] A.H. Hammad, M.A. Marzouk, H.A. ElBatal, The effects of Bi_2O_3 on optical, FTIR and thermal properties of SrO-B_2O_3 glasses, Silicon 8 (2016) 123–131, https://doi.org/10.1007/s12633-015-9283-x.

[38] N. Anu, Deopa, A.S. Rao, Structural and luminescence characteristics of thermally stable Dy^{3+} doped oxyfluoride strontium zinc borosilicate glasses for photonic device applications, Opt Laser. Technol. 154 (2022), 108328, https://doi.org/10.1016/j.optlastec.2022.108328.

[39] N. Jaidass, C. Krishna Moorthi, A. Mohan Babu, M. Reddi Babu, Luminescence properties of Dy^{3+} doped lithium zinc borosilicate glasses for photonic applications, Heliyon 4 (2018), e00555, https://doi.org/10.1016/j.heliyon.2018.e00555.

[40] L. Zhang, Q. Sun, J. Wang, Z. Zhang, W. Zhang, J. Wang, H. Chen, M. Li, Effect of SrO content on microstructure of Bi_2O_3-B_2O_3-ZnO-BaO-SrO low-melting glass frit and joining performance of sodalime glass substrates, J. Alloys Compd. 872 (2021), 159707, https://doi.org/10.1016/j.jallcom.2021.159707.

[41] G. El-Damrawi, A.k. Hassan, A. Shahboub, Characteristic studies on Ag_2O-Al_2O_3-P_2O_5 glasses and glass ceramics, Mater. Sci. Eng. B. 264 (2021), 114957, https://doi.org/10.1016/j.mseb.2020.114957.

[42] Y. Chen, Y. Zhao, F. Liu, M. Ding, J. Wang, J. Jiang, P. Boulet, M.-C. Record, Structural and electrochemical properties of Li_2O-V_2O_5-B_2O_3-Bi_2O_3 glass and glass-ceramic cathodes for lithium-ion batteries, Molecules 28 (2023) 229, https://doi.org/10.3390/molecules28010229.

[43] A. Okasha, S.Y. Marzouk, A.M. Abdelghany, Design a tunable glasses optical filters using CuO doped fluoroborate glasses, Opt Laser. Technol. 137 (2021), 106829, https://doi.org/10.1016/j.optlastec.2020.106829.

[44] A. Cosgun Ergene, S. Khabbaz Abkenar, A. Senol Gungor, E. Gunay, H. Kurt, G. Topcu, C.W. Ow-Yang, Oxide glass formers extending persistent luminescence in Eu and Dy co-doped strontium aluminates, J. Lumin. 257 (2023), 119719, https://doi.org/10.1016/j.jlumin.2023.119719.

[45] M.A. Ouis, M.A. Marzouk, Comparative optical, FTIR and photoluminescence spectral analysis of copper ions in BaO–B_2O_3, SrO–B_2O_3 or Bi_2O_3–B_2O_3 glasses and impact of gamma irradiation, J. Lumin. 223 (2020), 117242, https://doi.org/10.1016/j.jlumin.2020.117242.

[46] H.A. Alyousef, Z.A. Alrowaili, M. Saad, H. Al-Mohiy, A.A. Alshihri, K.S. Shaaban, M.S. Al-Buriahi, E.A.A. Wahab, Examinations of mechanical, and shielding properties of CeO_2 reinforced B_2O_3–ZnF_2–Er_2O_3–ZnO glasses for gamma-ray shield and neutron applications, Heliyon 9 (2023), e14435, https://doi.org/10.1016/j.heliyon.2023.e14435.

[47] A.J.A. Al-Nidawi, K.A. Matori, M.H.M. Zaid, J.Y.C. Liew, M.A.A. Khushaini, A.R.M. Zain, W.R.M. Mutage, M.A.M. Abuallan, A.M.E. Efa, Enhancement of elastic properties and surface plasmon resonance with the addition of boron oxide to the ZnO−SiO_2 glass system, J. Non-Cryst. Solids 605 (2023), 122175, https://doi.org/10.1016/j.jnoncrysol.2023.122175.

[48] B. Eraiah, Optical properties of lead-tellurite glasses doped with samarium trioxide, Bull. Mater. Sci. 33 (2010) 391–394, https://doi.org/10.1007/s12034-010-0059-z.

[49] L.W.X. Rebecca, Z.A. Burhanudin, M. Abdullah, M.S.M. Saheed, Structural changes and band gap tunability with incorporation of n-butylammonium iodide in perovskite thin film, Heliyon 6 (2020), e03364, https://doi.org/10.1016/j.heliyon.2020.e03364.

[50] A. Okasha, M.S. Gaafar, S.Y. Marzouk, The influence of concentration variation on the spectroscopic behavior of Sm^{3+}-doped zinc–lead-phosphates glasses for orange and reddish-orange light-emitting applications: experimental and Judd–Ofelt approach, J. Mater. Sci. Mater. Electron. 34 (2023) 354, https://doi.org/10.1007/s10854-022-09677-6.

[51] I. Abdullahi, S. Hashim, S.K. Ghoshal, Waveguide laser potency of samarium doped $BaSO_4$-TeO_2-B_2O_3 glasses: evaluation of structural and optical qualities, J. Lumin. 216 (2019), https://doi.org/10.1016/j.jlumin.2019.116686.

[52] M.A. Farag, A.A. Elbakey, M.K. El-Mansy, T.Y. Elrasasi, Judd–Ofelt and spectroscopic analysis of erbium ions co-doped with samarium ions in phosphate glasses environment, Opt. Quantum Electron. 55 (2023) 358, https://doi.org/10.1007/s11082-022-04317-z.

[53] I.S. Mahmoud, M.S. Gaafar, S.Y. Marzouk, Role of Sm^{+3} ions on structural, optical and radiation shielding properties of lead borosilicate glasses, J. Mater. Res. Technol. 13 (2021) 1032–1044, https://doi.org/10.1016/J.JMRT.2021.05.051.

[54] S.N. Fadhilah Zalamin, M.H. Mohd Zaid, K.A. Matori, M.K. Abdul Karim, N.A. Mohamad Yamin, N.A. Nazihah Ismail, Comprehensive study on optical and luminescence properties of Sm^{3+} doped magnesium borotellurite glasses, J. Phys. Chem. Solids. 163 (2022), 110563, https://doi.org/10.1016/J.JPCS.2021.110563.

[55] M.A. Ouis, W.M. Abd-Allah, O.I. Sallam, Gamma ray interaction with soda lime silicate glasses doped with V_2O_5, CuO or SrO, Appl. Phys. A. 128 (2022) 389, https://doi.org/10.1007/s00339-022-05522-z.

[56] B.R. Judd, Optical absorption intensities of rare-earth ions, Phys. Rev. 127 (1962) 750–761, https://doi.org/10.1103/PhysRev.127.750.

[57] G.S. Ofelt, Intensities of crystal spectra of rare-earth ions, J. Chem. Phys. 37 (1962) 511–520, https://doi.org/10.1063/1.1701366.

[58] S. Hashim, S.K. Ghoshal, I. Abdullahi, On the lasing potency of samarium-activated $BaSO_4$–TeO_2–B_2O_3 glass host : Judd – Ofelt analysis, Indian J. Phys. 94 (2020) 1811–1820, https://doi.org/10.1007/s12648-019-01631-3.

[59] I. Abdullahi, S. Hashim, G. S.K, L. Sa'ad, Modified structure and spectroscopic characteristics of Sm^{3+}/Dy^{3+} co-activated barium-sulfur-telluro-borate glass host: role of plasmonic gold nanoparticles inclusion, Opt Laser. Technol. 132 (2020), 106486.

[60] A. Mohammed Aliyu, R. Hussin, N.E. Ahmad, Y.A. Yamusa, Samarium doped calcium sulfate ultra-phosphate glasses: structural, physical and luminescence investigations, Optik 172 (2018) 1162–1171, https://doi.org/10.1016/j.ijleo.2018.07.123.

[61] S.Y. Marzouk, A.H. Hammad, Influence of samarium ions on the structural, and optical properties of unconventional bismuth glass analyzed using the Judd–Ofelt theory, J. Lumin. 231 (2021), 117772, https://doi.org/10.1016/j.jlumin.2020.117772.

[62] H. Largot, K.E. Aiadi, M. Ferid, S. Hraiech, C. Bouzidi, C. Charnay, K. Horchani-Naifer, Spectroscopic investigations of Sm^{3+} doped phosphate glasses: Judd-Ofelt analysis, Phys. B Condens. Matter 552 (2019) 184–189, https://doi.org/10.1016/j.physb.2018.10.010.

[63] P. Srivastava, S.B. Rai, D.K. Rai, Optical properties of Sm^{3+} doped calibo glass with addition of lead oxide, Spectrochim, Acta Part A Mol. Biomol. Spectrosc. 60 (2004) 637–642, https://doi.org/10.1016/S1386-1425(03)00273-7.

[64] I. Kashif, A. Ratep, The effect of replacing copper metal or oxide with neodymium on the optical properties of lithium tetraborate glass, J. Mater. Sci. Mater. Electron. 33 (2022) 19231–19241, https://doi.org/10.1007/s10854-022-08761-1.

[65] S.B. Kolavekar, N.H. Ayachit, R. Rajaramakrishna, P. N G, J. Kaewkhao, Reddish-orange emission and Judd-Ofelt investigation of Sm^{3+} ions doped in zinc-bismuth-phospho-tellurite glasses for solid lighting application, J. Lumin. 226 (2020), 117498, https://doi.org/10.1016/J.JLUMIN.2020.117498.

[66] V.M. Krishna, S. Mahamuda, P.R. Rani, K. Swapna, M. Venkateswarlu, A.S. Rao, Effect of samarium ions concentration on physical, optical and photoluminescence properties of Oxy-Fluoro Boro Tellurite glasses, Opt. Mater. 109 (2020), 110368, https://doi.org/10.1016/j.optmat.2020.110368.

[67] P. Pascuta, R. Stefan, L.E. Olar, L.C. Bolundut, E. Culea, Effects of copper metallic nanoparticles on structural and optical properties of antimony phosphate glasses co-doped with samarium ions, Materials 13 (2020) 1–11, https://doi.org/10.3390/ma13215040.

[68] J.A. Jiménez, Optical spectroscopy of Cu^{+}/Sm^{3+}-activated aluminophosphate glasses: effect of Cu^{2+} impurities on the Sm^{3+} photoluminescence enhancement, J. Alloys Compd. 623 (2015) 401–406, https://doi.org/10.1016/j.jallcom.2014.11.050.

[69] J.A. Jiménez, Samarium(III) as luminescent probe for copper(II), J. Lumin. 161 (2015) 352–357, https://doi.org/10.1016/j.jlumin.2015.01.037.

[70] G. Chandana, C. Nageswara Rao, P. Vasudeva Rao, M.J.S. Al-Musawi, K. Samatha, G.G. Dhar, Luminescent properties of Sm^{3+} doped metal fluoro phosphate glasses, Optik 208 (2020), 163909, https://doi.org/10.1016/J.IJLEO.2019.163909.

[71] I. Abdullahi, S. Hashim, S.K. Ghoshal, A.U. Ahmad, Structures and spectroscopic characteristics of barium-sulfur-telluro-borate glasses : role of Sm^{3+} and Dy^{3+} Co-activation, Mater. Chem. Phys. 247 (2020), 122862.

[72] S. Hashim, S.K. Ghoshal, I. Abdullahi, On the lasing potency of samarium-activated $BaSO_4$–TeO_2–B_2O_3 glass host : Judd – Ofelt analysis, Indian J. Phys. (2019), https://doi.org/10.1007/s12648-019-01631-3.

[73] I. Khan, M. Shoaib, N. Srisittipokakun, I. Ullah, A. Ahad, S. Kothan, G. Rooh, J. Kaewkhao, Spectroscopic investigation of Sm_2O_3-activated barium calcium strontium borate glasses for laser and display-devices applications, Optik 265 (2022), 169439, https://doi.org/10.1016/j.ijleo.2022.169439.

[74] V.B. Sreedhar, C. Basavapoornima, C.K. Jayasankar, Spectroscopic and fluorescence properties of Sm^{3+}-doped zincfluorophosphate glasses, J. Rare Earths 32 (2014) 918–926, https://doi.org/10.1016/S1002-0721(14)60163-0.

[75] S. Thomas, S.N. Rasool, M. Rathaiah, V. Venkatramu, C. Joseph, N.V. Unnikrishnan, Spectroscopic and dielectric studies of Sm^{3} + ions in lithium zinc borate glasses, J. Non-Cryst. Solids 376 (2013) 106–116, https://doi.org/10.1016/j.jnoncrysol.2013.05.022.

[76] M. Shoaib, G. Rooh, R. Rajaramakrishna, N. Chanthima, H.J. Kim, S. Tuscharoen, J. Kaewkhao, Physical and luminescence properties of samarium doped oxide and oxyfluoride phosphate glasses, Mater. Chem. Phys. 229 (2019) 514–522, https://doi.org/10.1016/j.matchemphys.2019.03.016.

[77] L. Yuliantini, R. Hidayat, M. Djamal, K. Boonin, P. Yasaka, E. Kaewnuam, Development of Sm^{3+} doped ZnO-Al_2O_3-BaO-B_2O_3 glasses for optical gain medium, J. Non-Cryst. Solids 482 (2018) 86–92, https://doi.org/10.1016/j.jnoncrysol.2017.12.012.

[78] M. Rajesh, E. Kavaz, B. D.P.R, Photoluminescence, radiative shielding properties of Sm^{3+} ions doped fluoroborosilicate glasses for visible (reddish-orange) display and radiation shielding applications, Mater. Res. Bull. 142 (2021), 111383, https://doi.org/10.1016/J.MATERRESBULL.2021.111383.

[79] I. Abdullahi, S. Hashim, S.K. Ghoshal, M.I. Sayyed, H.A. Thabit, N.N. Yusof, Enhanced up- and down-conversion luminescence from Dy^{3+}-Sm^{3+} co-doped B_2O_3-$SrCO_3$-TeO_2-Al_2O_3-MgO glass hosts: effects of CuO nanoparticles embedment, Phys. Scr. 98 (2023), 065511, https://doi.org/10.1088/1402-4896/acd152.